STRUCTURAL BIOLOGY COMMUNICATIONS

ISSN 2053-230X

Structural insights into the catalytic mechanism of *Bacillus subtilis* BacF

Ashish Deshmukh and Balasubramanian Gopal*

Molecular Biophysics Unit, Indian Institute of Science, Bangalore, Karnataka 560 012, India. *Correspondence e-mail: bgopal@iisc.ac.in

Received 1 October 2019
Accepted 5 February 2020

Edited by R. Sankaranarayanan, Centre for Cellular and Molecular Biology, Hyderabad, India

Keywords: transaminases; external aldimine; stereospecificity; enzyme catalysis; bacilysin synthesis.

PDB references: BacF, apo, 6l1l; substrate-bound, 6l1n; product-bound, 6l1o

Supporting information: this article has supporting information at journals.iucr.org/f

The nonribosomal biosynthesis of the dipeptide antibiotic bacilysin is achieved by the concerted action of multiple enzymes in the *Bacillus subtilis bac* operon. BacF (YwfG), encoded by the *bacF* gene, is a fold type I pyridoxal 5-phosphate (PLP)-dependent stereospecific transaminase. Activity assays with L-phenylalanine and 4-hydroxyphenylpyruvic acid (4HPP), a chemical analogue of tetrahydrohydroxyphenylpyruvic acid (H_4HPP), revealed stereospecific substrate preferences, a finding that was consistent with previous reports on the role of this enzyme in bacilysin synthesis. The crystal structure of this dimeric enzyme was determined in its apo form as well as in substrate-bound and product-bound conformations. Two ligand-bound structures were determined by soaking BacF crystals with substrates (L-phenylalanine and 4-hydroxyphenylpyruvate). These structures reveal multiple catalytic steps: the internal aldimine with PLP and two external aldimine conformations that show the rearrangement of the external aldimine to generate product (L-tyrosine). Together, these structural snapshots provide an insight into the catalytic mechanism of this transaminase.

1. Introduction

Bacilysin is a simple dipeptide antibiotic with an L-alanine residue at the N-terminus attached to a nonproteinogenic amino acid, L-anticapsin (Walker & Abraham, 1970*a*, 1970*b*). This antibiotic acts against a wide range of bacteria and fungi as it is a potent inhibitor of glucosamine-6-phosphate synthase. Bacilysin thus acts by disrupting cell-wall synthesis (Walton & Rickes, 1962). The nonribosomal biosynthetic pathway for the production of bacilysin has been well characterized by genetic studies as well as the *in vitro* analysis of several enzymes. These studies revealed that enzymes encoded by the polycistronic *bacA–F* operon and the monocistronic *bacG* gene are involved in bacilysin biosynthesis (Inaoka *et al.*, 2003; Mahlstedt & Walsh, 2010. In this biosynthetic pathway, BacA catalyzes the decarboxylation of prephenate and the specific isomerization of a pro-*R* double bond, leading to an endocyclic dienyl product: 7*R*-endocyclic dihydrohydroxyphenylpyruvate (H_2HPP; Mahlstedt & Walsh, 2010). BacB is an isomerase that transfers the double bond to a conjugate 2-keto moiety, leading to 3*E* and 3*Z* isomers of 7*R*-exocyclic H_2HPP (ex-H_2HPP; Rajavel *et al.*, 2009; Mahlstedt & Walsh, 2010; Parker & Walsh, 2012). BacC is an NAD^+-dependent alcohol dehydrogenase that oxidizes the C7 hydroxyl to form functional anticapsin (Parker & Walsh, 2013). BacD is a ligase that catalyzes the ligation of L-alanine with L-anticapsin to form bacilysin (Steinborn *et al.*, 2005; Tabata *et al.*, 2005; Shomura *et al.*, 2012; Parker & Walsh, 2013). These *in vitro* observations are consistent with mutational analysis, in which the addition

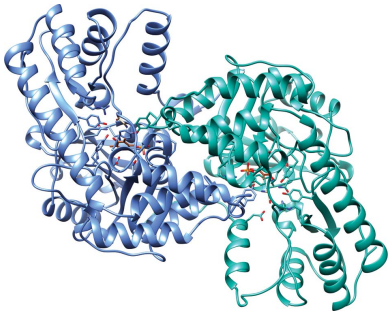

Table 1
Macromolecule-production information.

Source organism	*B. subtilis*
DNA source	*B. subtilis*
Forward primer	5′-CTAGCTAGCATGGAAATAACACCGTCC GA-3′
Reverse primer	5′-CCGCTCGAGTTAGCGGGATGTTTCTTG TAATG-3′
Cloning vector	pET-22b
Expression vector	pET-22b
Expression host	*E. coli* BL21 (DE3)
Complete amino-acid sequence of the construct produced	MEITPSDVIKTLPRQEFSLVFQKVKEMEKT GAHIINLGQGNPDLPTPPHIVEALREAS LNPSFHGYGPFRGYPFLKEAIAAFYKRE YGVTINPETEVALFGGGKAGLYVLTQCL LNPGDIALVPNPGYPEYLSGITMARAEL YEMPLYEENGYLPDFEKIDPAVLEKAKL MFLNYPNNPTGAVADAAFYAKAAAFAKE HNIHLIHDFAYGAFEFDQKPASFLEAED AKTVGAELYSFSKTFNMAGWRMAFAVGN EKIIQAVNEFQDHVFVGMFGGLQQAASA ALSGDPEHTESLKRIYKERIDFFTALCE KELGWKMEKPKGTFYVWAEIPNTFETSH QFSDYLLEHAHVVVTPGEIFGSNGKRHV RISMVSKQEDLREFVTRIQKLNLPFGSL QETSRHHHHHH

of purified BacC or BacD to the cell extracts from Δ*bacC* or Δ*bacD* strains revealed anticapsin formation and bacilysin production, respectively (Parker & Walsh, 2013). Subsequent experiments revealed that the C5—C6 double-bond epoxide was formed prior to the action of BacC (Parker & Walsh, 2013). BacE is the only membrane protein in the *bac* operon. The role of this protein is to pump out bacilysin from *Bacillus subtilis*. The mutation of *bacE* in *B. subtilis* GSB322 led to the inhibition of bacterial growth and to lysis of the culture, suggesting that accumulation of bacilysin within the cell is harmful to the host (Steinborn *et al.*, 2005). BacF has been shown to be an aminotransferase that converts H_4HPP to tetrahydrotyrosine (H_4Tyr) in the presence of the coenzyme pyridoxal 5-phosphate (PLP) (Mahlstedt & Walsh, 2010; Parker & Walsh, 2012). The other characterized enzyme in this enzymatic cascade is BacG (previously referred to as YwfH). BacG is an NADPH-dependent reductase that reduces 3*E* and 3*Z* ex-H_2HPP to 4*R*- and 4*S*-tetrahydrohydroxyphenylpyruvate (H_4HPP), respectively (Parker & Walsh, 2012; Rajavel *et al.*, 2013).

BacF has been suggested to be enantiospecific and to only act on L-phenylalanine (as a co-substrate), thereby ensuring *S* stereochemistry at the C2 position of H_4HPP (Parker & Walsh, 2012). In this study, which was performed using nuclear magnetic resonance spectroscopy and mass spectrometry, no product (H_4Tyr) was seen in the BacF reaction mixture when D-phenylalanine was used as a substrate (Parker & Walsh, 2012). These observations led to the suggestion that this class I PLP-dependent aspartate aminotransferase utilizes PLP as a cofactor to catalyze transamination by converting tetrahydrohydroxyphenylpyruvate (H_4HPP) to tetrahydrotyrosine using L-phenylalanine as a co-substrate (Mahlstedt & Walsh, 2010; Parker & Walsh, 2012). Here, we present the results of an activity assay of BacF with 4-hydroxyphenylpyruvic acid [4HPP; an analogue of tetrahydrohydroxyphenylpyruvic acid (H_4HPP)] and both enantiomers of phenylalanine, which reveals stereospecific substrate recruitment; a finding that is consistent with previous reports on this enzyme. We also describe crystal structures of *B. subtilis* BacF in its native and ligand-bound forms. The structures of this dimeric enzyme provide snapshots of different steps in catalysis. While the apo BacF structure reveals the presence of PLP in the internal aldimine form, the crystal structures of the ligand complexes depict the rearrangement of the external aldimine. Together, the biochemical and structural data reveal a conformational rationale for the catalytic mechanism of this enantiospecific transaminase.

Table 2
Crystallization.

Method	Microbatch
Plate type	72-well microbatch plate
Temperature (K)	295
Protein concentration (mg ml^{-1})	8
Buffer composition of protein solution	50 m*M* Tris pH 7.4, 250 m*M* NaCl, 1 m*M* DTT, 2 m*M* PMSF, 0.5 m*M* PLP
Composition of reservoir solution	0.1 *M* sodium acetate trihydrate, 0.1 *M* cacodylate trihydrate pH 6.5, 30%(*w*/*v*) polyethylene glycol 8000
Volume and ratio of drop	2 µl, 1:1
Volume of reservoir (µl)	10

2. Materials and methods

2.1. Purification and expression of BacF

The plasmid encoding the *bacF* gene was transformed into *Escherichia coli* BL21(DE3) cells to overexpress recombinant *B. subtilis* BacF. Briefly, the *E. coli* culture was grown in Luria–Bertani broth containing 100 µg ml^{-1} ampicillin at 37°C. At an OD of 0.5, BacF expression was induced by the addition of 0.3 m*M* isopropyl β-D-1-thiogalactopyranoside (IPTG). After subsequent growth at 18°C for 12 h, the cells were harvested by centrifugation and resuspended in buffer *A* [50 m*M* Tris–HCl pH 7.4, 250 m*M* NaCl, 2 m*M* phenylmethylsulfonyl fluoride (PMSF), 1 m*M* dithiothreitol (DTT), 0.5 m*M* PLP]. The *E. coli* cells were lysed by sonication (Ultrasonic Processor, model GEX-750) in pulse mode (on time, 2 s; off time, 6 s; pause, 4 min; on ice at 34% amplitude). The lysate was centrifuged at 14 000 rev min^{-1} in a Kubota centrifuge for 45 min. An immobilized metal-affinity chromatography (IMAC) step was used for the purification of recombinant BacF. The supernatant was then loaded onto an Ni^{2+}–NTA agarose column equilibrated with buffer *A* and eluted with a linear gradient of imidazole (30–300 m*M*) in buffer *A*. The pure BacF protein fractions were pooled and concentrated by centrifugation using a Millipore centrifugal Centricon (30 kDa). The purity of BacF was assessed by SDS–PAGE. Macromolecule-production information is summarized in Table 1.

2.2. Analytical size-exclusion chromatography

The oligomeric status of freshly purified BacF was evaluated by size-exclusion chromatography. These experiments

Table 3
Data-collection and processing statistics.

Values in parentheses are for the outer shell.

	Apo BacF	Substrate-bound BacF	Product-bound BacF
Diffraction source	BM14, ESRF	BM14, ESRF	21-ID-D, APS
Wavelength (Å)	0.9537	0.9840	0.9791
Temperature (K)	100	100	100
Detector	MAR Mosaic 225 CCD	MAR Mosaic 225 CCD	PILATUS3 6M
Crystal-to-detector distance (mm)	242.19	205.35	280.14
Rotation range per image (°)	0.5	0.5	0.5
Total rotation range (°)	210	300	180
Exposure time per image (s)	6	6	6
Space group	$P12_11$	$P12_11$	$P12_11$
a, b, c (Å)	73.22, 59.44, 84.23	71.29, 56.91, 78.5	73.89, 59.19, 85.81
α, β, γ (°)	90, 101.78, 90	90, 97.86, 90	90, 103.39, 90
Mosaicity (°)	1.11	0.65	1.12
Resolution range (Å)	82.46–1.95 (2.02–1.95)	77.9–1.97 (2.037–1.967)	83.48–1.85 (1.916–1.850)
R_{merge}	0.130 (0.628)	0.077 (0.279)	0.081 (0.522)
R_{meas}	0.158 (0.768)	0.084 (0.305)	0.098 (0.633)
Total No. of reflections	157341 (22967)	279659 (39593)	178317 (26036)
No. of unique reflections	51644 (7568)	44675 (6470)	58705 (8742)
Completeness (%)	99.40 (100.00)	99.96 (99.66)	94.98 (97.66)
Multiplicity	3.0 (3.0)	6.3 (6.1)	3.0 (2.9)
$\langle I/\sigma(I)\rangle$	5.5 (2.0)	14.8 (5.6)	7.6 (2.1)
$CC_{1/2}$	0.981 (0.606)	0.997 (0.946)	0.994 (0.786)
Overall B factor from Wilson plot (Å^2)	22.78	21.17	24.81

Table 4
Structure-solution and refinement statistics.

Values in parentheses are for the outer shell.

	Apo BacF	Substrate-bound BacF	Product-bound BacF
Resolution range (Å)	82.46–1.95 (2.02–1.95)	77.9–1.97 (2.04–1.97)	83.48–1.85 (1.92–1.85)
Completeness (%)	99.40 (100.00)	99.96 (99.66)	94.98 (97.66)
No. of reflections, working set	48980	42490	55713
No. of reflections, test set	2508	2169	2886
Final R_{cryst}	0.2244 (0.3279)	0.1755 (0.2047)	0.1832 (0.2608)
Final R_{free}	0.2693 (0.3628)	0.2271 (0.2763)	0.2341 (0.3167)
Cruickshank DPI	0.227	0.203	0.159
No. of non-H atoms			
Protein	5989	5958	6063
Ligand	0	20	28
Water	347	308	406
Total	6336	6286	6497
R.m.s. deviations			
Bonds (Å)	0.016	0.018	0.019
Angles (°)	1.77	1.83	1.85
Average B factors (Å^2)			
Overall	28.90	24.30	27.30
Protein	28.60	24.00	26.80
Ligand	—	24.80	24.90
Water	34.20	30.90	35.00
Ramachandran plot			
Most favoured (%)	97	97	98
Outliers (%)	0	0.13	0.26

were performed using a Superdex 200 10/300 GL column (24 ml column volume; GE Healthcare) equilibrated in 50 m*M* Tris–HCl buffer containing 200 m*M* NaCl. The flow rate was set to 0.3 ml min^{-1} for these experiments.

2.3. Spectroscopic assay for BacF activity

As the UV absorption spectra of the reactants and products of BacF have a substantial overlap, we monitored the catalytic activity of BacF at 295 nm, where the difference in absorbance is the most significant. UV absorption measurements were performed using a JASCO V-530 spectrophotometer. A typical reaction was monitored for 20 min at room temperature. The reaction mixture consisted of 150 n*M* BacF, 0.5 m*M* L-phenylalanine and 5–200 µ*M* 4HPP in 50 m*M* Tris–HCl buffer containing 200 m*M* NaCl. Each reading in the Michaelis–Menten plot corresponds to an average of three independent measurements. To evaluate the substrate stereospecificity of BacF, the reaction was performed with 0.5 m*M* L- or D-phenylalanine along with 0.2 m*M* 4HPP.

2.4. Crystallization and diffraction data collection

Crystallization trials were performed using the microbatch method with the crystallization condition and BacF in a 1:1 ratio by volume. BacF crystals were obtained in 0.1 *M* sodium acetate trihydrate, 0.1 *M* sodium cacodylate trihydrate pH 6.5, 30%(*w*/*v*) polyethylene glycol 8000. To determine the substrate-bound structure of BacF, apo BacF crystals were soaked with 5 m*M* L-phenylalanine substrate (dissolved in the crystallization condition) and 10%(*v*/*v*) ethylene glycol for 1 h prior to flash-cooling in liquid nitrogen. For the structure of product-bound BacF, crystals were incubated in a solution consisting of the crystallization condition, 10% ethylene glycol and 5 m*M* each of L-phenylalanine and 4-hydroxyphenylpyruvic acid for 1 h. Crystallization information is summarized in Table 2. Diffraction data for apo BacF and ligand-soaked BacF crystals were collected under cryogenic conditions (100 K) with an oscillation of 0.5° per image on the BM-14 beamline at the European Synchrotron Radiation Facility (ESRF), Grenoble and at the Advanced Photon Source (APS), Argonne National Laboratory. The diffraction data were processed using *iMosflm* (Battye *et al.*, 2011) and scaled using *SCALA* (Evans, 2006). We note that the crystal of substrate-bound BacF (apo BacF crystals soaked with L-phenylalanine) has a lower mosaicity when compared with the crystals of apo BacF or product-bound BacF (apo BacF crystals soaked with L-phenylalanine and 4-hydroxyphenylpyruvic acid). Initial phases were obtained by molecular replacement (MR) using the crystal structure of *Staphylococcus aureus* transaminase (PDB entry 2o1b; T. E. McGrath, A. Dharamsi, D. Thambipillai, A. M. Edwards, E. F. Pai & N. Y. Chirgadze, unpublished work), which shares 39.8% sequence identity with *B. subtilis* BacF, as a search model. MR calculations performed using *Phaser* (Read, 2001) provided easily interpretable electron-density maps. The solution had an LLG of 381, an RFZ of 8.7 and a TFZ of 20.8. Refinement of the rebuilt model was performed using *REFMAC*5 (Murshudov *et al.*, 2011), while the fit of the model to the electron density was evaluated using *Coot* (Emsley *et al.*, 2010). The diffraction data, refinement and model statistics are reported in Tables 3 and 4.

3. Results and discussion

In bacteria, the last step in the synthesis of the aromatic amino acids phenylalanine and tyrosine is the aminotransferase-catalyzed amination of the precursors phenylpyruvate and

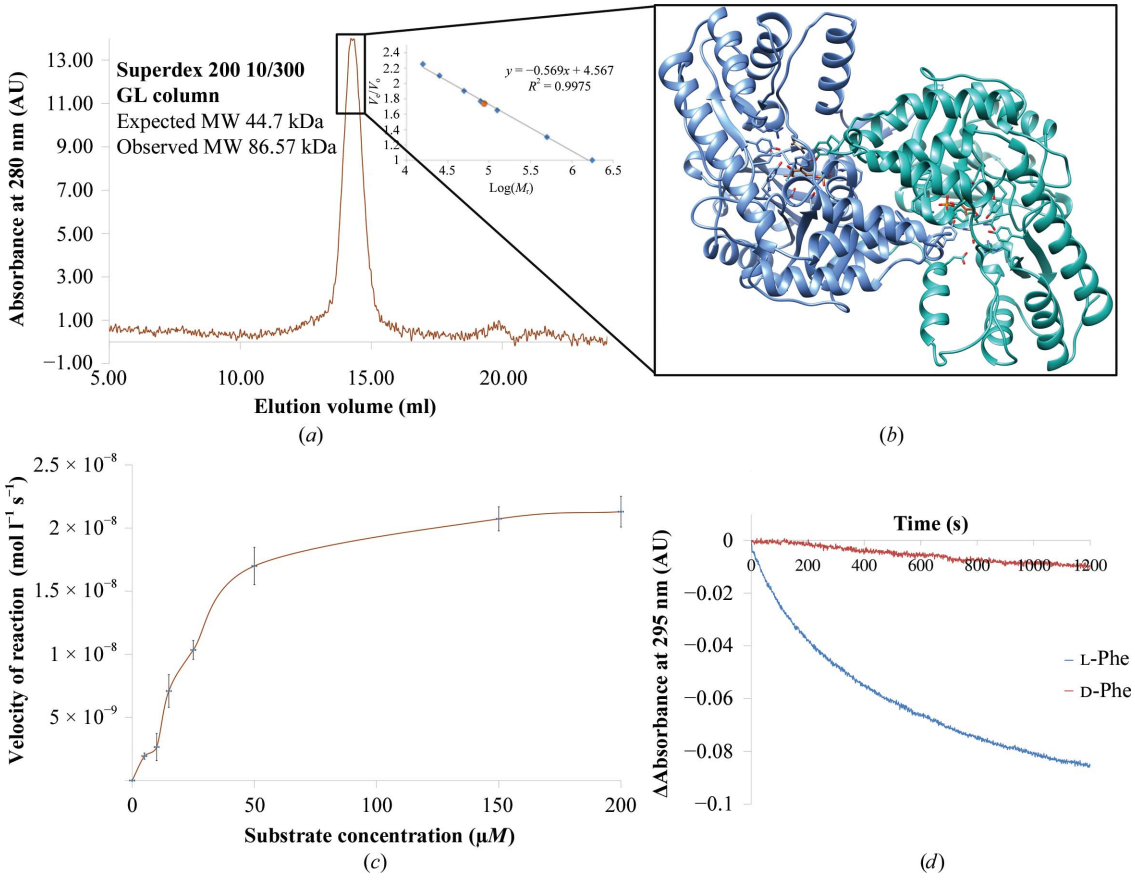

Figure 1
B. subtilis BacF is a dimer in solution and in the crystal. (*a*) An analytical size-exclusion chromatogram reveals that BacF is a dimer in solution. (*b*) The asymmetric unit of the monoclinic crystal form reported in this manuscript contains a dimer of BacF. (*c*) Enzyme assays reveal enantioselective substrate recruitment. The transamination reaction of BacF was monitored using 4-hydroxyphenylpyruvic acid (4HHP), a chemical analogue of H_4HPP. As the λ_{max} of the reactants and products overlap, we monitored the reaction at 295 nm, where the difference in absorbance between the reactants and products is significant.

p-hydroxyphenylpyruvate (Berry *et al.*, 1987). Glutamate is the amino donor in this reaction (Fischer *et al.*, 1993; Prakash *et al.*, 2005). The pathway for bacilysin synthesis branches off at a later stage in the synthesis of aromatic amino acids (Roscoe & Abraham, 1966; Hilton *et al.*, 1988). Substantial insights have been obtained from genetic studies, leading to the identification of the genes that are involved in this biosynthetic pathway and thus leading to a plausible enzymatic route for bacilysin synthesis that could be tested *in vitro*. Nevertheless, two significant lacunae still persist in our understanding of this biosynthetic pathway. The first involves the identification of an epoxidase, while the second is the step in the enzyme cascade where stereospecificity is enforced in the synthesis of the nonproteogenic amino acid anticapsin. The crystal structure(s) of *B. subtilis* BacF address the latter aspect by providing a structural rationale for stereospecific substrate recruitment.

In general, PLP-dependent enzymes of fold type I exist either as a homodimer or a homotetramer in solution (Han *et al.*, 2010; Milano *et al.*, 2013). Analytical size-exclusion chromatography experiments performed on freshly purified *B. subtilis* BacF revealed a dimer (~88 kDa; Fig. 1). Indeed, dimerization is an obligatory feature of transaminases as the active site is located at the interface of two monomeric units. In the monoclinic crystal form reported here, the BacF dimer

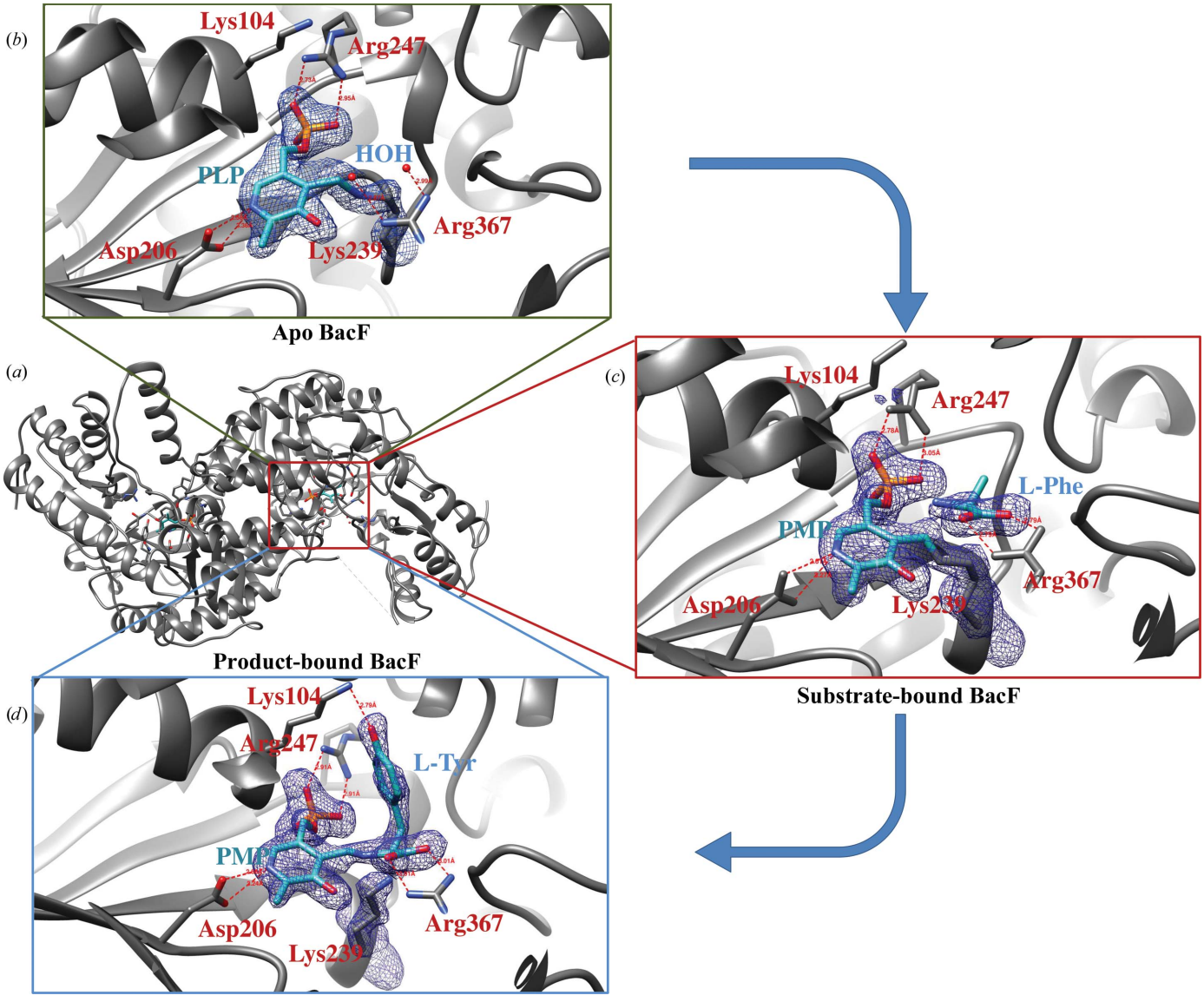

Figure 2
Structural snapshots of distinct steps in the catalytic mechanism of *B. subtilis* BacF. (*a*) The catalytic site is highlighted in the crystal structure of the BacF dimer. (*b*) Experimental electron-density maps of the BacF active-site cavity in the apo form. Consistent with spectroscopic measurements, electron density corresponding to the internal aldimine was seen in the ($mF_o - DF_c$) experimental electron-density map. (*c*) The second distinct step (referred to as external aldimine 1) is shown. A glycine residue could be modelled in the electron-density map. This conformation reveals a Schiff base via covalent bonding between the bound substrate and PMP. This structure was obtained from BacF crystals soaked with L-phenylalanine. (*d*) Electron density corresponding to a product, L-tyrosine, could be modelled in this structure. L-Tyrosine replaces three structured water molecules that could be modelled in the apo BacF structure.

in the asymmetric unit is also the biologically relevant conformation of this enzyme (Fig. 1). In this structural arrangement, each subunit consists of two domains. As in other fold type I transaminases, a β-sheet forms the core of the structure. This broad overall structural feature is retained in this family of enzymes. Significant differences between homologues are thus restricted to loops or the substrate-binding pocket (Schneider *et al.*, 2000). The crystal structure of BacF is consistent with this observation.

BacF is *S*-specific (Parker & Walsh, 2012). Another observation that was made during the course of these studies was that BacF selectively recruits L-phenylalanine (2*S*) as an amino donor along with the co-substrate H_4HPP that is produced by other enzymes in the Bac biosynthetic pathway. In this study, activity assays were performed using 4-hydroxyphenylpyruvic acid [4HPP; an analogue of tetrahydrohydroxyphenylpyruvic acid (H_4HPP)] and both enantiomers of phenylalanine (Fig. 1). These assays unambiguously suggested stereospecific substrate recruitment, with the corollary that similar stereospecificity would be enforced for the partner keto acid (L-phenylalanine) that is reductively aminated by the transaminase. The activity assay thus validated the use of 4HPP as a suitable substrate analogue for structural analysis.

Crystal structures of *B. subtilis* BacF were determined in three distinct catalytic steps (Fig. 2). As is the case in this class of PLP-dependent enzymes, the multistep catalytic mechanism of BacF can be broadly depicted in terms of two distinct half-cycles. The first involves an internal aldimine. Freshly purified BacF was yellow, suggesting that the recombinant enzyme had bound PLP. The internal aldimine [recognized as a covalent bond between imino (>NH) and carbonyl (>C═O) groups] absorbs at ∼408 nm, while unbound PLP absorbs at ∼388 nm. Indeed, the UV absorption spectrum of BacF suggested an internal aldimine. The unambiguous electron density allowed us to model the internal aldimine along with PLP in the case of the apo (no substrate) BacF structure. This is the first structural 'snapshot' in Fig. 2(*b*). The validity of the model built for this complex was evaluated using OMIT map calculations. In the substrate-free (apo form) of BacF, the ε-amino group of the conserved Lys239 forms a Schiff-base linkage with the aldehyde group of PLP. This structure suggests that PLP is stabilized at the active site by interaction with neighbouring residues (Tyr209, Asp206, Arg247, Asn174, Tyr325, Tyr128 and Tyr209) and π-stacking with the side chain of Tyr128.

The catalytic mechanism in all PLP enzymes has an imine-exchange step involving the amino group of the substrate and the lysine ε-amino group in a Schiff-base linkage. Catalysis is

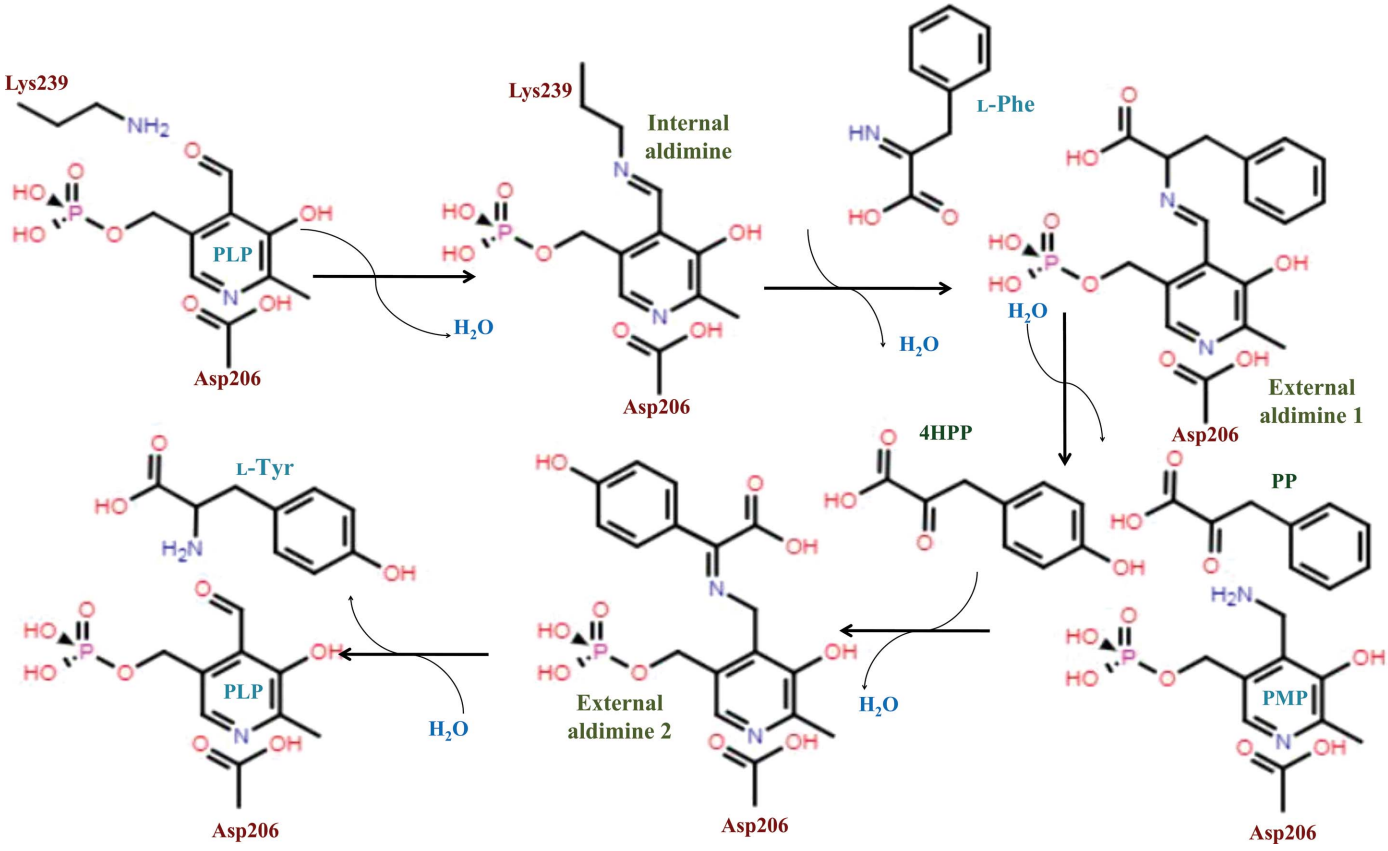

Figure 3
Schematic of the reaction catalysed by BacF. The first step involves PLP binding. The apo BacF structure with the internal aldimine represents the activated form of the enzyme (PDB entry 6l1l). Binding of the substrate (L-phenylalanine) leads to the external aldimine 1 state, as depicted by the crystal of substrate-bound BacF (PDB entry 6l1n). The product-bound form represented by the structure with L-tyrosine at the active site is a shapshot of the external aldimine 2 state (PDB entry 6l1o).

initiated upon the transfer of the substrate amino group to PLP, leading to a pyridoxamine enzyme (PMP) and a keto product. This step in the catalytic cycle facilitates the delocalization of the negative charge of the PLP-bound substrate. Subsequently, the amino group of PMP is transferred to a keto (or aldehyde) acceptor, yielding an amine and regenerating PLP in the pyridoxal form (Fig. 3). In crystallization trials to obtain the substrate-bound structure, the electron density near the PLP-binding site corresponds to the substrate (L-phenylalanine in this soaking experiment). The side chain of L-phenylalanine could not be modelled in this structure owing to poor electron density (Fig. 2*c*). Alternate models were evaluated for the electron density at this site, including an acetate ion. The experimental electron density, however, could be best modelled as an amino acid, with a real-space correlation coefficient (RSCC) of 0.94. In this intermediate 'substrate-bound conformation', the Michaelis complex state depicts the first half-reaction of the catalytic process. In this step, the internal aldimine is converted into an external aldimine, in which the substrate amine forms a Schiff-base linkage with the cofactor (PMP), releasing the side-chain ε-amino group of the lysine. The third structure, with electron density for L-tyrosine at the active site, represents the ketimine intermediate (Fig. 2*d*) that is formed through protonation of the former aldehyde C atom of the coenzyme. In general, since different intermediates can be generated from the quinonoid by transfer of protons, the residues in the active site determine the substrate specificity and the type of PLP-dependent reaction that is catalyzed. The BacF structure shows that L-tyrosine can be covalently linked to PMP (Fig. 2*d*) and hence is chemically involved in catalysis. The reaction catalysed in this case involves the conversion of *S*-4HPP to L-tyrosine. This structure also suggests a rationale for the stereospecificity. The binding of *R*-4HPP at this site is likely to be structurally stabilized by interaction with neighbouring residues (Tyr325 and Tyr209), making it a less suitable substrate. The enforcement of stereospecificity in fold type I transaminases is thus best exemplified in the external aldimine structural descriptions of BacF.

Together, the structural snapshots of BacF reveal features of the catalytic mechanism that enforce stereoselectivity and direct the type of PLP-dependent reaction (Fig. 3). The structures also suggest that BacF could be a rate-limiting step in the biosynthetic pathway to bacilysin production. The structural insights into the different catalytic steps of transamination by BacF are likely to provide a basis for repurposing or engineering this enzyme for other substrates that might be significant from a biotechnological perspective or in therapeutic applications.

Funding information

This work was funded in part by a grant from the DBT–IISc partnership program. The X-ray facility is funded by an IRHPA grant (DST–SERB) and the XRD2 beamline is funded by a grant from the DST, India. Funding from the DST–FIST and Infosys Foundation for research facilities is gratefully acknowledged. AD is a UGC Senior Research Fellow.

References

Battye, T. G. G., Kontogiannis, L., Johnson, O., Powell, H. R. & Leslie, A. G. W. (2011). *Acta Cryst.* D**67**, 271–281.
Berry, A., Ahmad, S., Liss, A. & Jensen, R. A. (1987). *J. Gen. Microbiol.* **133**, 2147–2154.
Emsley, P., Lohkamp, B., Scott, W. G. & Cowtan, K. (2010). *Acta Cryst.* D**66**, 486–501.
Evans, P. (2006). *Acta Cryst.* D**62**, 72–82.
Fischer, R. S., Bonner, C. A., Boone, D. R. & Jensen, R. A. (1993). *Arch. Microbiol.* **160**, 440–446.
Han, Q., Ding, H., Robinson, H., Christensen, B. M. & Li, J. (2010). *PLoS One*, **5**, e8826.
Hilton, M. D., Alaeddinoglu, N. G. & Demain, A. L. (1988). *J. Bacteriol.* **170**, 482–484.
Inaoka, T., Takahashi, K., Ohnishi-Kameyama, M., Yoshida, M. & Ochi, K. (2003). *J. Biol. Chem.* **278**, 2169–2176.
Mahlstedt, S. A. & Walsh, C. T. (2010). *Biochemistry*, **49**, 912–923.
Milano, T., Paiardini, A., Grgurina, I. & Pascarella, S. (2013). *BMC Struct. Biol.* **13**, 26.
Murshudov, G. N., Skubák, P., Lebedev, A. A., Pannu, N. S., Steiner, R. A., Nicholls, R. A., Winn, M. D., Long, F. & Vagin, A. A. (2011). *Acta Cryst.* D**67**, 355–367.
Parker, J. B. & Walsh, C. T. (2012). *Biochemistry*, **51**, 5622–5632.
Parker, J. B. & Walsh, C. T. (2013). *Biochemistry*, **52**, 889–901.
Prakash, P., Pathak, N. & Hasnain, S. E. (2005). *J. Biol. Chem.* **280**, 20666–20671.
Rajavel, M., Mitra, A. & Gopal, B. (2009). *J. Biol. Chem.* **284**, 31882–31892.
Rajavel, M., Perinbam, K. & Gopal, B. (2013). *Acta Cryst.* D**69**, 324–332.
Read, R. J. (2001). *Acta Cryst.* D**57**, 1373–1382.
Roscoe, B. J. & Abraham, E. P. (1966). *Biochem. J.* **99**, 793–800.
Schneider, G., Käck, H. & Lindqvist, Y. (2000). *Structure*, **8**, R1–R6.
Shomura, Y., Hinokuchi, E., Ikeda, H., Senoo, A., Takahashi, Y., Saito, J., Komori, H., Shibata, N., Yonetani, Y. & Higuchi, Y. (2012). *Protein Sci.* **21**, 707–716.
Steinborn, G., Hajirezaei, M. R. & Hofemeister, J. (2005). *Arch. Microbiol.* **183**, 71–79.
Tabata, K., Ikeda, H. & Hashimoto, S. (2005). *J. Bacteriol.* **187**, 5195–5202.
Walker, J. E. & Abraham, E. P. (1970*a*). *Biochem. J.* **118**, 557–561.
Walker, J. E. & Abraham, E. P. (1970*b*). *Biochem. J.* **118**, 563–570.
Walton, R. B. & Rickes, E. L. (1962). *J. Bacteriol.* **84**, 1148–1151.